

Original Research

Copper Overload Promotes β -amyloid Induced NLRP3/Caspase-1/GSDMD-Mediated Pyroptosis in Alzheimer's Disease

Min-Juan Zhu¹, Ling Zhang^{2,3}, Chang-Peng Wang^{4,*}

Academic Editor: Andrei Surguchov

Submitted: 9 May 2024 Revised: 5 July 2024 Accepted: 18 July 2024 Published: 21 October 2024

Abstract

Purpose: Alzheimer's disease (AD) is characterized by cognitive decline and abnormal protein accumulation. Copper imbalance and pyroptosis play significant roles in the pathogenesis of AD. Recent studies have suggested that dysregulated copper homeostasis contributed to β -amyloid accumulation, which may activate the NOD-like receptor protein 3 (NLRP3)-related pyroptosis pathway, promoting neuronal damages and AD progression. Therefore, the present study aims to investigates whether copper facilitates AD through exacerbating β -amyloid (A β) induced activation of NLRP3/Caspase-1/Gasdermin D (GSDMD)-mediated neuronal cell pyroptosis. **Methods**: Mouse hippocampal HT-22 cells were cultured with $A\beta$ 1-42 oligomer for 24 h as AD Model group. CuCl₂ treatment was administered to the AD cell model, and cell survivability levels were detected by Cell Counting Kit-8 (CCK-8), TdT-mediated dUTP nick end labeling (TUNEL), and other relevant kits. Mitochondrial function was evaluated using Mitochondrial membrane potential dye JC-1 and transmission electron microscopy (TEM). After intervention with the NLRP3 inhibitor MCC950, activation of the NLRP3/Caspase-1/GSDMD pathway by copper ions (Cu²⁺) was confirmed via Western Blot. Thioredoxin T (ThT) fluorescence assay was performed to observe the aggregation effect of $A\beta$ induced by Cu^{2+} overload. **Results**: $CuCl_2$ treatment of the AD cell model resulted in upregulation of the levels of Lactate Dehydrogenase (LDH), Interleukin-1 β (IL-1 β), and IL-18 expression, which indicated activation of pyroptosis. We observed a significant decrease in mitochondrial membrane potential, mitochondrial swelling, and loss of mitochondrial cristae by fluorescence microscopy and TEM. ThT fluorescence imaging showed that Cu^{2+} promoted A β aggregation and up-regulated NLRP3, apoptosis-associated speck-like protein containing a CARD (ACS), Caspase-1, Cleaved Caspase-1, GSDMD, and Gasdermin D N-terminal (GSDMD-NT). The NLRP3 inhibitor MCC950 partially reversed Cu²⁺-mediated pyroptosis in HT-22 cells. Conclusions: Exposure to copper ions disrupt mitochondrial copper homeostasis, promotes $A\beta$ aggregation, and activates NLRP3 inflammasomes, further promoting the A β aggregation activated pyroptosis in AD cell models.

Keywords: copper overload; $A\beta$; NLRP3; neuron; pyroptosis

1. Introduction

Alzheimer's disease (AD) is a common progressive neurodegenerative disease. The clinical manifestations of AD include continuous cognitive and memory decline, reduced ability to perform daily living activities, and a variety of neuropsychiatric symptoms and behavioral disorders [1,2]. Abnormal accumulation of β -amyloid (A β), neural protofibrillary tangles (NFTs) composed of highly phosphorylated tau proteins, neuronal loss, and neuroinflammatory responses are the basic features of AD [3,4].

Accumulative studies have indicated the critical role of copper in various cellular processes, particularly in mitochondrial function, metabolic reprogramming, and cancer biology, indicating the vital function of coppermitochondrial homeostasis in various diseases [5–11]. Proteomics revealed protein targets and pathways in AD that are significantly altered by copper-induced and oxidative

modifications, which are related to the mitochondria dysfunction [6]. Recent studies focusing on the effects of metal ions on AD also determined the abnormal accumulation of copper ions (Cu^{2+}), indicating that copper level might be one of the pathological factors of AD pathogenesis [7,8]. Elevated levels of Cu^{2+} may result in the aggregation of $A\beta$, the binding of apolipoprotein E (APOE), and the increase of reactive oxygen species [9,10]. Moreover, copper exposure may induce $A\beta$ aggregation promoting NOD-like receptor protein 3 (NLRP3)-mediated neurotoxicity, highlighting the role of copper in mediating pyroptosis [11].

Pyroptosis is a novel mode of cell death triggered by activated inflammatory vesicles, of which the inflammatory vesicles are represented by the NOD-like receptor (NLR) family [12]. $A\beta$ triggers the onset of cellular pyroptosis by activating NLRP3 inflammatory vesicles in neurons, microglia, and astrocytes [12,13]. And apoptosis-associated

¹Neurology Department, Shanghai General Hospital, Shanghai Jiao Tong University School of Medicine, 200080, Shanghai, China

 $^{^2\}mathrm{Neurology}$ Department, Shanghai Xuhui Central Hospital, 200041 Shanghai, China

 $^{^3\}mbox{Neurology}$ Department, Zhongshan-Xuhui Hospital, Fudan University, 200437 Shanghai, China

⁴Department of Neurovascular Intervention, Shanghai General Hospital, Shanghai Jiao Tong University School of Medicine, 200080 Shanghai, China

^{*}Correspondence: zj230125@163.com (Chang-Peng Wang)

speck-like protein containing a CARD (ASC) in the inflammatory vesicle complex promotes the aggregation of $A\beta$ protein in the brain, which in turn exacerbates AD pathology [11]. Therefore, the aim of this study was to investigate copper overload exacerbates $A\beta$ aggregation and activation of NLRP3/Caspase-1/Gasdermin D (GSDMD)-mediated neuronal cell pyroptosis.

2. Materials and Methods

2.1 Reagents

Mouse hippocampal cell HT-22 (CL-039m, American Type Culture Collection (ATCC), Manassas, VA, USA). Dulbecco's modified Eagle's medium (DMEM) and Trypsin (12491015 and 25200072, Gibco, Grand Island, NE, USA). PBS buffer, Ammonium persulfate substitute, Radio-immunoprecipitation assay buffer (RIPA), Phenylmethylsulfonyl fluoride (PMSF), Sodium dodecyl sulfate (SDS), Tetramethylethylenediamine (TEMED), and TdT-mediated dUTP nick end labeling (TUNEL) assay kit (C0221A, ST005, P0013B, ST505, ST626, ST728, and C1088, Beyotime, Shanghai, China). 30% Acr/Bic, Tris-Base, Triton X-100, TBS buffer (BL513B, BS083-500g, BS084-1000ml, BL600A, Biosharp, Hefei, SDS, Glycine, skimmed milk (3250KG001, China). 1275KG2P5, Biofroxx GmbH, Guangzhou, China). Bicinchoninic acid (BCA) protein assay kit, 5× Sodium dodecyl sulfate polyacrylamide gel electrophoresis buffer (5× SDS-PAGE) buffer, Enhanced chemiluminescence luminescent solution A and B (ECL luminescent solution AB) (WB6501, P2010, P10300, NCM Biotech, Suzhou, Western Antibody Diluent, Glyceraldehyde-3-phosphate dehydrogenase (GAPDH)-Loading Control (bsm-33033M, Bioss, Beijing, China), Goat anti-rabbit immunoglobulin g heavy and light chain/horseradish peroxidase (IgG H&L/HRP) (bs-0295G-HRP, Bioss, Beijing, China), Goat anti-mouse IgG H&L/HRP (bs-0296G-HRP, Bioss, Beijing, China), Anti-NLRP3 antibody (EPR23094-1) (ab263899, Abcam, Cambridge, UK), Anti-tumor necrosis factor receptor-associated signal transducer (TMS1)/Apoptosis-Associated Speck-Like Protein Containing a CARD (ASC) antibody (RM1049) (ab309497, Abcam, Cambridge, UK), Anti-Caspase-1 antibody (EPR19672) (ab207802, Abcam, Cambridge, UK), Cleaved-Caspase 1 antibody (HY-P80622, MedChemExpress, Monmouth Junction, NJ, USA), Anti-Gasdermin D (GSDMD) antibody (EPR20859) (ab219800, Abcam, Cambridge, UK), Anti-cleaved N-terminal GSDMD (GSDMD-NT) antibody (EPR20829-408) (ab215203, Abcam, Cambridge, UK), Mouse Interleukin- 1β (IL- 1β) Enzyme Linked Immunosorbent Assay (ELISA) kit (SEKM-0002, Solarbio, Beijing, China), Mouse IL-18 ELISA Kit (SEKM-0019, Solarbio, Beijing, China), Cell Counting Kit-8 (CCK-8) cell proliferation assay Kit (BA00208, Bioss, Beijing, China). Lactate Dehydrogenase (LDH)

Assay Kit, Mitochondrial Membrane Potential Assay Kit (JC-1 method) (ml095184, ml094797, Sigma-Aldrich, St. Louis, WI, USA).

2.2 Experimental Apparatus

Ultra-low temperature refrigerator (DW-86L626, Haier, Qingdao, China). Optical microscope (XSP-2800, Shanghai Optical Instrument No.1 Factory, Shanghai, China). CO₂ cell incubator, ultra-clean bench, constant temperature water bath (BC-J80, BSC-1000B2, SSW-420-2S, Shanghai BoXun Industrial Medical Equipment Factory, Shanghai, China). Ultra-pure water meter (ELGA Veoli, Paris, France). Real-time fluorescence quantitative polymerase chain reaction (PCR) instrument (CFX96 Touch 1855195, Bio-Rad, Hercules, CA, USA), Western blotting system CriterionTM electrophoresis tank+Transblot® transfer tank (1658033, Bio-Rad, Hercules, CA, USA). EVOS M5000 fluorescence microscope (AMF5000, Themo Fisher, Waltham, MA, USA). Orbital shaker TS-100 (E0020, Kylin-Bell, Haimen, China). chemiluminescence analyzer (ZF-368, Shanghai Jiapeng Technology Co., Ltd., Shanghai, China).

2.3 Cell Culture and Processing

The HT-22 cell line has been meticulously certified through analysis and has successfully passed routine mycoplasma contamination tests, with the outcome being negative. The HT-22 cells were cultured in DMEM supplemented with 10% FBS+1% P/S. When the cells reached 80%–90%, PBS was used for washing. Digestion was terminated by adding 2 mL of 0.25% trypsin-0.02% Ethylene-diaminetetraacetic acid (EDTA, ST1303-250g, Beyotime, Shanghai, China) mixture and 6 mL of complete medium. Cells were resuspended after centrifugation for cell counting and plate spreading.

Routinely cultured HT-22 cells were used as controls. HT-22 cells were cultured with 10 μM concentration of A β 1-42 oligomer for 24 h as Model group according to previously published methods [14]. L-CuCl $_2$ group was constructed by culturing HT-22 with 5 μM CuCl $_2$ and 10 μM A β 1-42 oligomer for 24 h, while the H-CuCl $_2$ group adjusted the CuCl $_2$ concentration to 30 μM [15,16]. HT-22 cells were cultured with 30 μM CuCl $_2$ and 10 μM A β 1-42 oligomer for 24 h, and then treated with 1.0 μM MCC950 for 30 min to construct H-CuCl $_2$ +NLRP3 inhibitor group.

2.4 TUNEL Assay for the Occurrence of Pyroptosis

HT-22 cells were seeded into 24-well plates with cell crawlers at a density of 1×10^4 cells/well. Cells were fixed with 1 mL of 4% paraformaldehyde and washed with PBS. TUNEL assay was prepared and added to the fixed cell wells, incubated at 37 °C for 60 min. Cells were washed with PBS, 100 μL of 4′,6-diamidino-2-phenylindole (DAPI, C1002, Beyotime, Shanghai, China) was added, incubated at room temperature and observed under a fluorescence microscope.



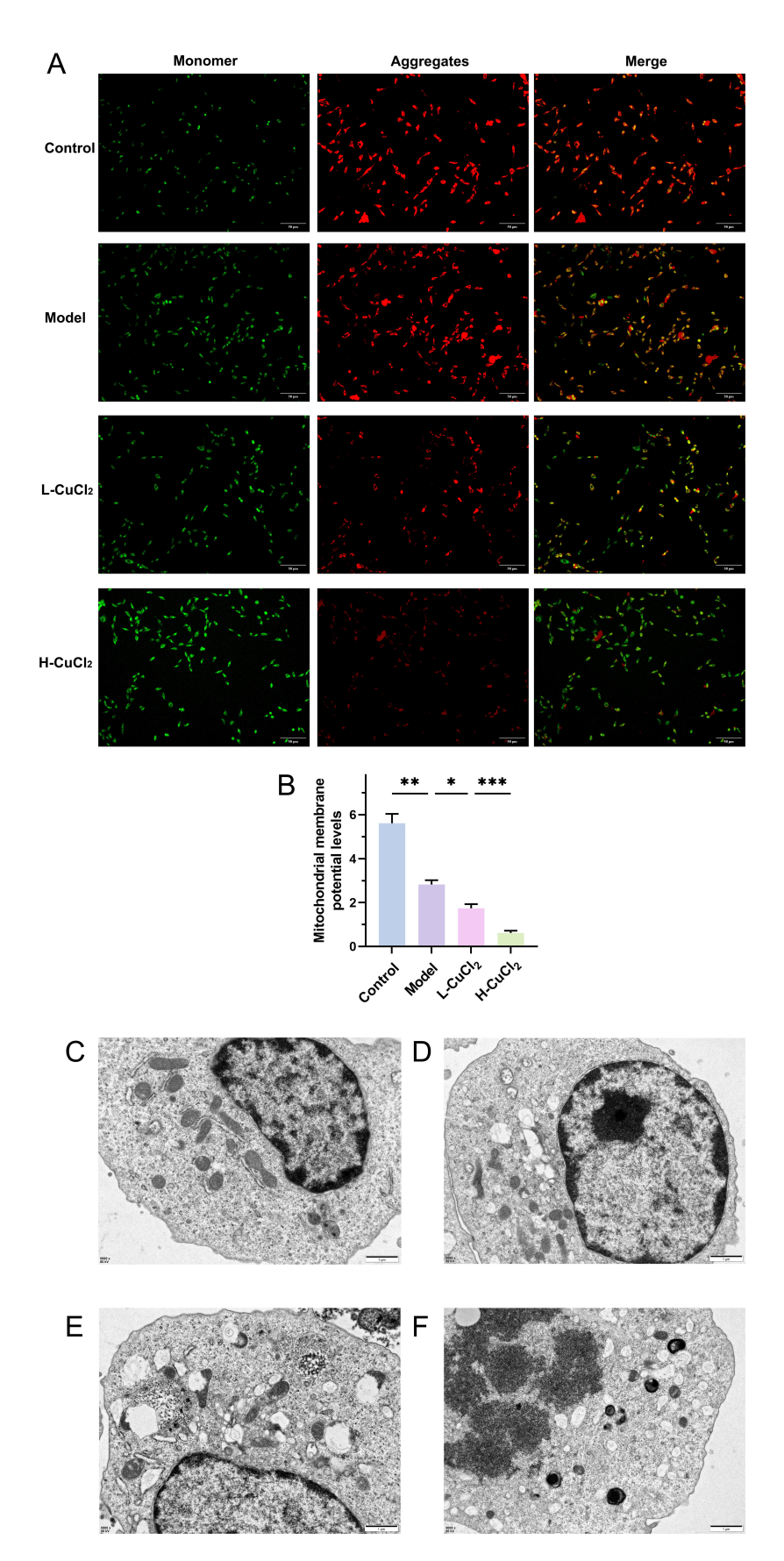


Fig. 1. The mitochondrial membrane potential and cell pyroptosis morphology in HT-22 cells were detected by JC-1 staining. (A) fluorescent images, (B) histogram. Transmission electron microscopy (TEM) images of (C) Control, (D) Model, (E) L-CuCl₂, and (F) H-CuCl₂. A: scale bar = 50 μ m, C-F: scale bar = 1 μ m. *p < 0.05, **p < 0.01, ***p < 0.001, n = 3.

2.5 Detection of Mitochondrial Membrane Potential by JC-1 Staining

HT-22 cells were seeded into 24-well plates with cell inserts at a density of 1×10^4 cells per well. 1 mL of JC-1 staining working solution was added to HT-22 cells and incubated at 37 °C for 20 min. Subsequently, 2 mL of cell culture medium containing serum and phenol red was added and observed under fluorescence microscope (AMF5000, Themo Fisher).

2.6 LDH Kit to Detect Extracellular LDH Release

HT-22 cells in the logarithmic growth phase were seeded into 96-well plates at a density of 2000 cells per well. Maximum enzyme activity control wells were added with LDH release reagent. 120 μL of supernatant from each well was taken and 60 μL of LDH assay working solution was added, and the absorbance was measured at 490 nm.

2.7 Detection of IL-1\beta, IL-18 Expression Levels by ELISA

The supernatant of HT-22 cells in each group was collected, and the standard was prepared according to the instructions of the ELISA kit. The sample was added 50 μL and incubated at 37 $^{\circ}C$ for 30 min. After washing, the enzyme-labeled reagent was added and the absorbance of each hole was measured at 450 nm.

2.8 CCK-8 Assay for Cell Viability

HT-22 cells were seeded at a density of 2000 cells per well into 96-well plates with 100 μ L of medium. Cells were cultured in 5 % CO₂, 37 °C for 24 h. 10 μ L CCK-8 solution was added to each well and incubated for 2 hours. Absorbance was measured at 450 nm with an enzyme marker.

2.9 Thioredoxin T (ThT) Fluorescent Staining Method

HT-22 cells were seeded at a density of 1×10^4 cells per well in fresh medium and incubated at 37 °C for 24 h. After the incubation, cells were treated according to each subgroup for another 24 h. The cells fixed and were stained with Thioredoxin T (THT, 596200, Sigma-Aldrich, St. Louis, MO, USA) solution and then observed by fluorescence microscope (AMF5000, Themo Fisher). The excitation wavelength (Em) used in this experiment is 450–500 nm, and the emission wavelength (Ex) is 515–565 nm.

2.10 Western Blot Detection of Protein Expression

Total protein was extracted with RIPA lysate and protein quantification was performed by BCA method. Proteins were separated via SDS-PAGE gel electrophoresis and transferred to a Polyvinylidene fluoride (PVDF) membrane (ISEQ00010, Millipore, Burlington, MA, USA). The membranes were then closed with 5% skimmed milk for 2 h at room temperature and incubated with NLRP3, ASC, Caspase-1, Cleaved Caspase-1, GSDMD, Gasdermin D Nterminal (GSDMD-NT) primary antibody at 4 °C overnight and incubated by secondary antibody. The membranes

were developed with a chemiluminescent imaging system and analyzed in grayscale with ImageJ Verson2 software (Bethesda, Rockville, MD, USA). In this experiment, 1.0 mm 10-well gel, 12% separation glue and 5% concentration glue were used. The electrophoresis conditions were 80 V 20 min and 120 V 45 min, respectively. The membrane transfer condition was 200 mA in ice water bath for 90 min. The original figures of Western Blot can be found in the **Supplementary Materials**.

2.11 Statistical Analysis

Data were analyzed and plotted using Graphpad Prism 9 (Version 9.4.0) (GraphPad Software, San Diego, CA, USA). AI was used to organize the combined graphs. All data were expressed as means \pm standard deviation (SD), and statistical differences between groups were tested using the T-Test or One-way test, with p values less than 0.05 considered significant.

3. Results

3.1 Copper Overload Mediates Mitochondrial Dysfunction in HT-22 Cells

To verify the effect of copper overload on the mitochondrial function in HT-22 cells, we first used JC-1 to detect mitochondrial membrane potential. As shown in Fig. 1A,B, the mitochondrial membrane potential was significantly lower in the AD model group compared to the Control group (p < 0.01). When the cells were treated with Cu²⁺, the mitochondrial membrane potential decreased significantly with an increase in Cu^{2+} concentration (p < 0.05). We then observed the submicroscopic mitochondrial structure of HT-22 cells by transmission electron microscopy (TEM). As shown in Fig. 1C–F, the mitochondria in the Control group were structurally intact with clear mitochondrial cristae. In the AD model group, nuclear chromatin was aggregated and mitochondria were swollen. After HT-22 cells were treated with Cu²⁺, the nuclear membrane was disrupted, intracellular vesicles were increased, mitochondria were swollen and mitochondrial cristae disappeared. The degree of damage increased with increasing Cu²⁺ concentration and the overall cells showed pyroptosis morphology. These results suggest that copper overload mediates the mitochondrial dysfunction and pyroptosis of HT-22 cells.

3.2 Copper Overload Promotes Pyroptosis in HT-22 Cells

To investigate the effects of copper overload on the AD model of HT-22 cells, we detected the cell death, LDH, IL-1 β and IL-18 levels of HT-22 cells in each group by TUNEL staining, LDH activities kit, and ELISA kit (Fig. 2A,B). The results indicated a significant increase in cellular death in the AD model (p < 0.01), with Cu²⁺ treatment further enhancing HT-22 death (p < 0.01). Next, LDH levels were measured in each group using an LDH assay kit. As shown in Fig. 2C, the Mode group exhibited signif-



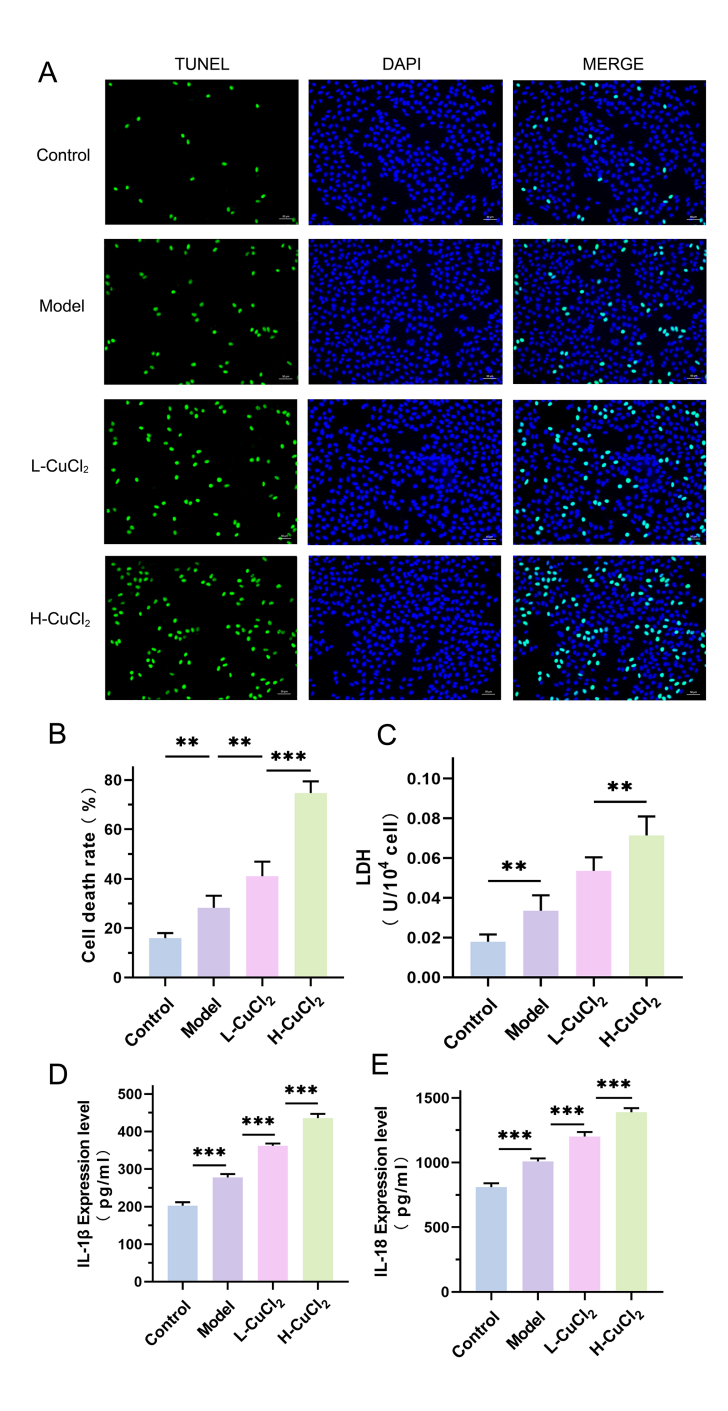


Fig. 2. Cell death markers and inflammatory factors were detected. The occurrence of cell death was detected by TUNEL staining (A) fluorescent images, (B) histogram. (C) Lactate Dehydrogenase (LDH) levels were detected by LDH kit. The levels of IL-1 β (D) and IL-18 (E) were detected by ELISA. A: scale bar = 50 μ m. **p < 0.01, ***p < 0.001, n = 3. ELISA, Enzyme Linked Immunosorbent Assay; TUNEL, TdT-mediated dUTP nick end labeling; IL, Interleukin; DAPI, 4',6-diamidino-2-phenylindole.

icantly elevated LDH levels compared to the Control group (p < 0.01). Moreover, increasing Cu^{2+} concentrations correlated with higher LDH levels in HT-22 cells (p < 0.01). Finally, the levels of IL-1 β and IL-18 in HT-22 cells were assessed by ELISA. Fig. 2D,E demonstrated that the AD model group had increased levels of the inflammatory cytokines IL-1 β and IL-18 compared to the Control group (p < 0.001). Cu^{2+} intervention in the AD model further ele-

vated the expression of IL-1 β and IL-18 (p < 0.001), with the H-CuCl₂ group showing significantly higher levels than in the L-CuCl₂ group (p < 0.001). These findings suggest that copper overloadpromotes pyroptosis like cell death in HT-22 cells.



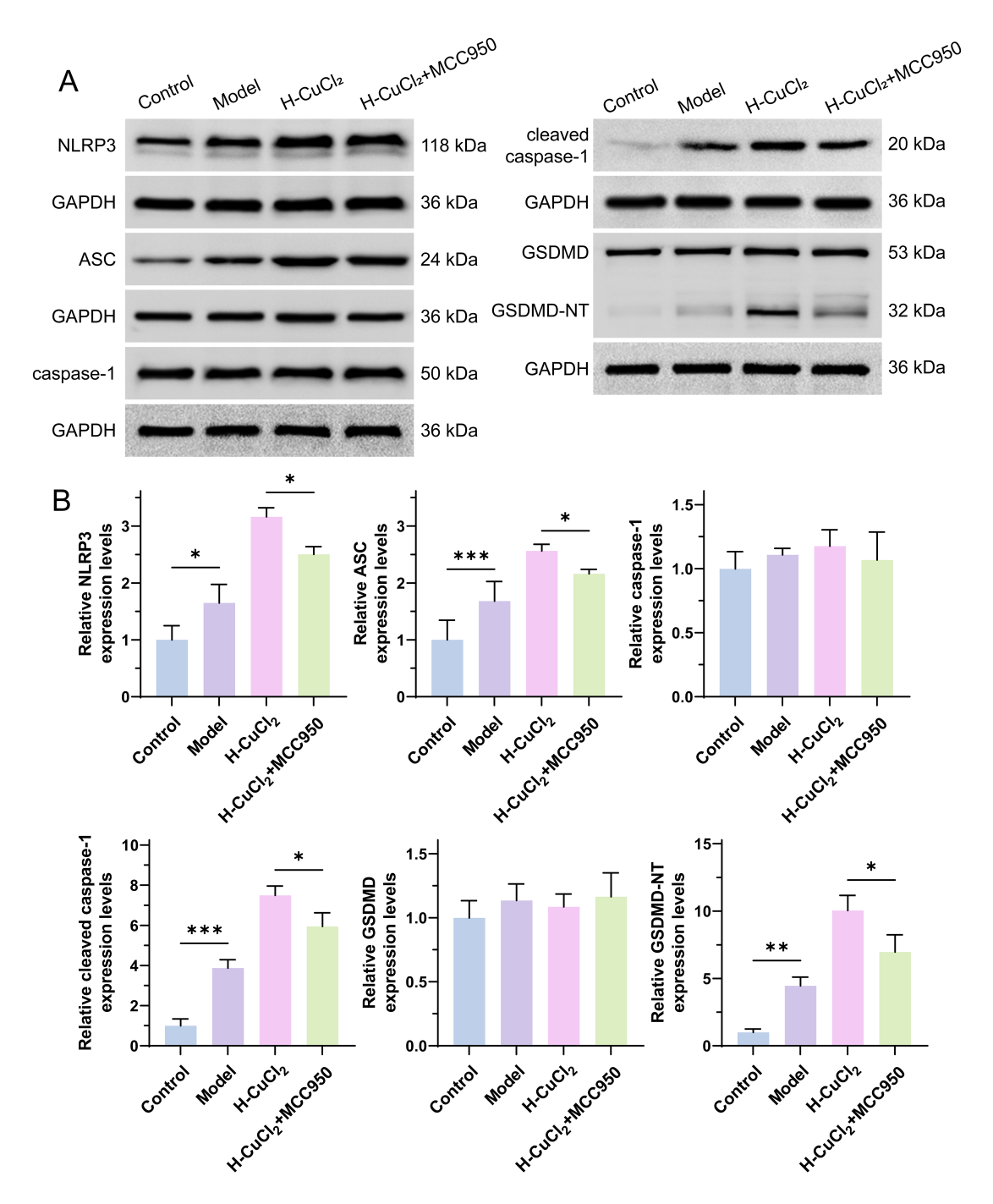


Fig. 3. Pyroptosis related proteins were detected. (A) Western blot assay for the protein expression levels of NLRP3, ASC, Caspase-1, Cleaved Caspase-1, GSDMD, and GSDMD-NT. (B) Quantitative analysis of the protein expression levels of NLRP3, ASC, Caspase-1, Cleaved Caspase-1, GSDMD, and GSDMD-NT. $^*p < 0.05$, $^{**}p < 0.01$, $^{***}p < 0.001$, $^{**}p < 0.001$, *

3.3 Copper Overload Mediates Pyroptosis via Activation of the NLRP3/Caspase-1/GSDMD Pathway in HT-22 Cells

To verify the activating cell death of Cu²⁺ was pyroptosis in HT-22 cells, we detected pyroptosis pathway proteins by Western Blot. As shown in Fig. 3, Cleaved Caspase-1 and GSDMD-NT expression was not detected in the Control group. However, the expression levels of

NLRP3, ASC, Cleaved Caspase-1, and GSDMD-NT were all significantly in the AD model of HT-22 cells (p < 0.05). Moreover, NLRP3, ASC, Cleaved Caspase-1, and GSDMD-NT expression levels were further up-regulated in the AD model incubated with high concentrations of Cu²⁺ (p < 0.05). These effects were significantly reversed by the NLRP3 inhibitor MCC950 (p < 0.05). The results demon-



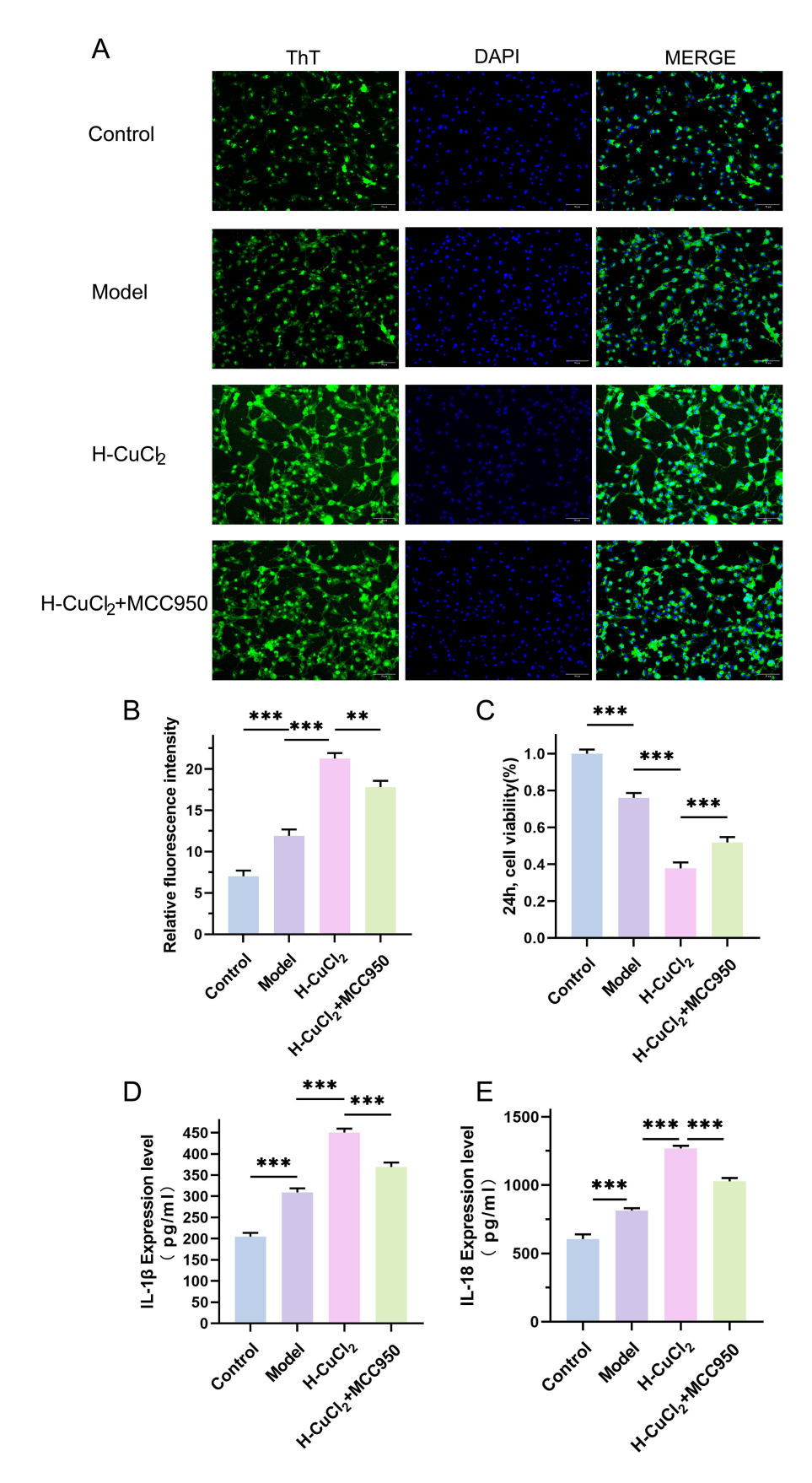


Fig. 4. Thioflavin T (THT) fluorescence staining was used to observe the aggregation of β -amyloid (A β). (A) fluorescent images, (B) histogram. (C) Cellular activity was detected by Cell Counting Kit-8 (CCK-8) assay. The levels of IL-1 β (D) and IL-18 (E) were detected by ELISA. A: scale bar = 50 μ m. **p < 0.01, ***p < 0.001, n = 3.

strated that copper overload mediated cell death through activation of the NLRP3/Caspase-1/GSDMD pathway mediated pyroptosis.

3.4 Copper Overload Promotes $A\beta$ Aggregation to Mediate Pyroptosis in HT-22 Cells

To investigate how copper overload aggravates pyroptosis in the AD model of HT-22 cells, we observed $A\beta$ aggregation using THT fluorescence staining (Fig. 4A,B). Compared to the control, the fluorescence level was significantly increased (p < 0.001), representing a significant increase in the degree of $A\beta$ aggregation in the model group. Treatment with a high concentration of Cu²⁺ further elevated the fluorescence intensity (p < 0.001). However, the addition of NLRP3 inhibitor MCC950 partially decreased the fluorescence intensity of A β (p < 0.01). Subsequently, the cell viability of each group was assayed using CCK-8 assay (Fig. 4C). Compared to the Control group, the cell viability was significantly decreased in the Model group (p < 0.001). Cell viability was further diminished after Cu²⁺ treatment (p < 0.001), but was partly restored when the pyroptosis pathway was inhibited by MCC950 (p < 0.001). As shown in Fig. 4D,E, after constructing the AD model, the expression levels of IL-1 β and IL-18 were significantly increased (p < 0.001). The levels of both were significantly increased after the intervention with a high concentration of Cu^{2+} in the AD model (p < 0.001). When the pyroptosis pathway was inhibited by MCC950, IL-1 β and IL-18 expression levels were partially downregulated (p < 0.001). These results suggest that copper overload promotes $A\beta$ aggregation, which mediates pyroptosis and inflammatory response.

4. Discussion

Copper is an essential trace element in human physiological system [17]. The brain is abundant in mitochondria, serving as a "copper reservoir", which is crucial for cellular activities; consequently, it boasts the highest copper content among all organs [18]. When the intracellular copper concentration surpasses the threshold maintained by the homeostatic mechanism, it exerts toxic effects on the cells. This can directly impact neural development and energy metabolism, ultimately leading to severe neurological damage [19]. Study has indicated that serum copper levels in AD patients were approximately 54% higher than those in healthy individuals, suggesting the potential value of copper levels as a peripheral blood marker for oxidative stress in distinguishing AD [20]. In the present study, we observed that Cu²⁺ treatment downregulated mitochondrial membrane potential and exacerbated mitochondrial damage in the AD model of HT-22 cells. At the same time, pyroptosis in HT-22 cells was observed by TUNEL staining, and the expression levels of the pyroptosis markers LDH, IL- 1β , and IL-18 were upregulated. These findings indicated

that copper overload contributed to the occurrence of pyroptosis in the AD model of HT-22 cells, in accordance with previous findings [21].

 $A\beta$ peptides possess a specific copper-binding site, and the abnormally accumulated copper directly binds to these peptides with high affinity. This interaction promotes the deposition and aggregation of $A\beta$, leading to neuronal damage, apoptosis, and dysregulation of neuronal synapses [22,23]. Altered copper ion concentrations influence the development of neuroinflammation in AD. Copper exposure has been shown to induce NLRP3dependent cellular pyroptosis and mediating neurotoxicity [24]. Dong et al. [24] used CuCl₂ in combination with lipopolysaccharide to treat primary microglial cells derived from non-mutant control mice, finding that the levels of NLRP3, Cleaved Caspase-1, ASC, and IL- 1β proteins were elevated in a time-dependent manner. Here, we also verified by western blotting that copper overload promoted pyroptosis through activation of the NLRP3/Caspase-1/GSDMD pathway. When the pyroptosis pathway was inhibited by MCC950, A β aggregation was significantly suppressed, HT-22 cell activity was significantly upregulated, and the expressions of inflammatory factors were significantly downregulated. Compared with the improvement of NLRP3 on copper exposure mediated neuroinflammatory damage, NLRP3 activation was also observed in aluminum-exposed mouse models and HT-22 [25], suggesting that NLRP3 inhibitors may have a potential role in the treatment of neuroinflammation. Notably, NLRP inhibitors were only able to partially reverse damage caused by copper exposure in HT-22 cells, suggesting that other transcription factors are involved in neuroinflammation in AD. These results suggested that copper exposure triggers an NLRP3 activation-mediated inflammatory response and neurotoxicity in neuronal cells. This demonstrates that excessive copper ion exposure may exacerbate disease progression in AD by promoting inflammatory responses in nerve cells.

5. Conclusions

In conclusion, we explored the effects of copper overload on A β aggregation, mitochondrial damage and pyroptosis in an AD model of HT-22 cells. We also verify the NLRP3/Caspase-1/GSDMD pathway is activated by copper overload, which further promotes the injury of HT-22 cells. However, it is important to note that this study has certain limitations. This study was conducted to explore the underlying mechanism in the HT-22 cell line, which may be of great relevance to the development of AD. Therefore, in vivo experiments are needed to further verify the mechanism by which copper exposure promotes $A\beta$ aggregation is our next step. This study revealed the pathological mechanisms of copper overload during AD development. Further studies may focus on the potential interactions between copper homeostasis and AD progression in animal and clinical investigations.



Availability of Data and Materials

The datasets used and/or analyzed during the current study are available from the corresponding author on reasonable request.

Author Contributions

Conceptualization: MJZ, CPW; Methodology: MJZ, LZ, CPW; Formal analysis and investigation: MJZ, LZ, CPW; Writing—original draft preparation: MJZ; Writing—review and editing: CPW; Funding acquisition: CPW; Supervision: CPW. All authors contributed to editorial changes in the manuscript. All authors read and approved the final manuscript. All authors have participated sufficiently in the work and agreed to be accountable for all aspects of the work.

Ethics Approval and Consent to Participate

Not applicable.

Acknowledgment

Not applicable.

Funding

The present study was supported by the Interdisciplinary Program of Shanghai Jiao Tong University (No. YG2021QN89) from Chang-Peng Wang.

Conflict of Interest

The authors declare no conflict of interest.

Supplementary Material

Supplementary material associated with this article can be found, in the online version, at https://doi.org/10.31083/j.jin2310194.

References

- [1] Scheltens P, De Strooper B, Kivipelto M, Holstege H, Chételat G, Teunissen CE, *et al.* Alzheimer's disease. Lancet. 2021; 397: 1577–1590.
- [2] Yin JT, Xu XW, Jin CY, Yuan XY, Wang XG. The Influence of the Gut Microbiota on Alzheimer's Disease: A Narrative Review. Journal of Integrative Neuroscience. 2023; 22: 38.
- [3] Tiwari S, Atluri V, Kaushik A, Yndart A, Nair M. Alzheimer's disease: pathogenesis, diagnostics, and therapeutics. International Journal of Nanomedicine. 2019; 14: 5541–5554.
- [4] Chen G, Han M, Chen Y, Lei Y, Li M, Wang L, et al. Danggui-Shaoyao-San Promotes Amyloid-β Clearance through Regulating Microglia Polarization via Trem2 in BV2 Cells. Journal of Integrative Neuroscience. 2023; 22: 72.
- [5] Ruiz LM, Libedinsky A, Elorza AA. Role of Copper on Mitochondrial Function and Metabolism. Frontiers in Molecular Biosciences. 2021; 8: 711227.
- [6] Tassone G, Kola A, Valensin D, Pozzi C. Dynamic Interplay between Copper Toxicity and Mitochondrial Dysfunction in Alzheimer's Disease. Life. 2021; 11: 386.
- [7] Sensi SL, Granzotto A, Siotto M, Squitti R. Copper and Zinc

- Dysregulation in Alzheimer's Disease. Trends in Pharmacological Sciences. 2018; 39: 1049–1063.
- [8] Li X, Chen X, Gao X. Copper and cuproptosis: new therapeutic approaches for Alzheimer's disease. Frontiers in Aging Neuroscience. 2023; 15: 1300405.
- [9] Singh SK, Balendra V, Obaid AA, Esposto J, Tikhonova MA, Gautam NK, *et al.* Copper-mediated β-amyloid toxicity and its chelation therapy in Alzheimer's disease. Metallomics: Integrated Biometal Science. 2022; 14: mfac018.
- [10] Stancu IC, Cremers N, Vanrusselt H, Couturier J, Vanoosthuyse A, Kessels S, et al. Aggregated Tau activates NLRP3-ASC inflammasome exacerbating exogenously seeded and non-exogenously seeded Tau pathology in vivo. Acta Neuropathologica. 2019; 137: 599–617.
- [11] Zhang Y, Gao H, Zheng W, Xu H. Current understanding of the interactions between metal ions and Apolipoprotein E in Alzheimer's disease. Neurobiology of Disease. 2022; 172: 105824.
- [12] Yu P, Zhang X, Liu N, Tang L, Peng C, Chen X. Pyroptosis: mechanisms and diseases. Signal Transduction and Targeted Therapy. 2021; 6: 128.
- [13] Moonen S, Koper MJ, Van Schoor E, Schaeverbeke JM, Vandenberghe R, von Arnim CAF, *et al.* Pyroptosis in Alzheimer's disease: cell type-specific activation in microglia, astrocytes and neurons. Acta Neuropathologica. 2023; 145: 175–195.
- [14] Chen WP, Zhang G, Cheng ZJ, Gu XH, Li M, Liu X. Inhibitor Kappa B Kinase β, Modulated by DJ-1/p-VHL, Reduces Phosphorylated Tau (p-Tau) Accumulation via Autophagy in Alzheimer's Disease Model. Neuroscience. 2021; 452: 1–12.
- [15] Shi W, Zhang H, Zhang Y, Lu L, Zhou Q, Wang Y, et al. Coexposure to Fe, Zn, and Cu induced neuronal ferroptosis with associated lipid metabolism disorder via the ERK/cPLA2/AA pathway. Environmental Pollution. 2023; 336: 122438.
- [16] Lu Q, Zhang Y, Zhao C, Zhang H, Pu Y, Yin L. Copper induces oxidative stress and apoptosis of hippocampal neuron via pCREB/BDNF/ and Nrf2/HO-1/NQO1 pathway. Journal of Applied Toxicology. 2022; 42: 694–705.
- [17] Cilliers K. Trace element alterations in Alzheimer's disease: A review. Clinical Anatomy. 2021; 34: 766–773.
- [18] Patel R, Aschner M. Commonalities between Copper Neurotoxicity and Alzheimer's Disease. Toxics. 2021; 9: 4.
- [19] Gromadzka G, Tarnacka B, Flaga A, Adamczyk A. Copper Dyshomeostasis in Neurodegenerative Diseases-Therapeutic Implications. International Journal of Molecular Sciences. 2020; 21: 9259.
- [20] Squitti R, Lupoi D, Pasqualetti P, Dal Forno G, Vernieri F, Chiovenda P, et al. Elevation of serum copper levels in Alzheimer's disease. Neurology. 2002; 59: 1153–1161.
- [21] An Y, Li S, Huang X, Chen X, Shan H, Zhang M. The Role of Copper Homeostasis in Brain Disease. International Journal of Molecular Sciences. 2022; 23: 13850.
- [22] Zhu X, Liu W, Zhao W, Chang Z, Yang J. The co-effect of copper and lipid vesicles on $A\beta$ aggregation. Biochimica et Biophysica Acta. Biomembranes. 2023; 1865: 184082.
- [23] Omar SH, Scott CJ, Hamlin AS, Obied HK. Olive Biophenols Reduces Alzheimer's Pathology in SH-SY5Y Cells and APPswe Mice. International Journal of Molecular Sciences. 2018; 20: 125.
- [24] Dong J, Wang X, Xu C, Gao M, Wang S, Zhang J, et al. Inhibiting NLRP3 inflammasome activation prevents copper-induced neuropathology in a murine model of Wilson's disease. Cell Death & Disease. 2021; 12: 87.
- [25] Zhu X, Hao W, Liu Z, Song Y, Hao C, Wu S, et al. Aluminum induces neuroinflammation via P2X7 receptor activating NLRP3 inflammasome pathway. Ecotoxicology and Environmental Safety. 2023; 249: 114373.

